Steady, Two-Dimensional, Natural Convection in Rectangular Enclosures With Differently Heated Walls

K. S. Chen

J. R. Ho

Department of Mechanical Engineering,
National Sun Yat-Sen University,
Kaohsiung, Taiwan 800,
Republic of China

J. A. C. Humphrey

Department of Mechanical Engineering,
University of California,
Berkeley, CA 94720
Mem. ASME

Numerical results are presented for steady natural convection in two-dimensional rectangular enclosures in which the side walls, top wall, and bottom wall are at uniform temperatures θ_s, θ_t, and θ_b, respectively, and $\theta_s > \theta_t > \theta_b$. Rayleigh numbers ranging from 10^4 to 10^7 and aspect ratios of 1 and 1.5 were investigated. The top wall was modeled as an impermeable rigid surface or an impermeable free-moving boundary. The calculations reveal two flow regions. In the upper part of the enclosure two large counterrotating cells appear, separated by a descending plume of fluid. Near the bottom wall the flow is almost motionless and stably stratified. The temperature in the central portion of the enclosure is almost uniform due to mixing by the recirculating cells. A temperature inversion occurs near the top wall and is particularly noticeable at high Rayleigh numbers. At high Rayleigh numbers the flow breaks up into smaller cells. The result is that each main recirculation region develops a secondary counterrotating eddy within it. The condition of a free surface as the top wall boundary condition significantly affects the circulation and heat transfer throughout the flow domain. Numerical experiments reveal the extent to which the flow field in the enclosure is affected by an asymmetric specification of side-wall temperature boundary conditions.

1 Introduction

It has been recognized that the growth of single crystals by the Czochralski technique (Hurle, 1977) is influenced by the fluid dynamics and heat transport characteristics of the process. The flow in the melt, due to natural convection, surface tension gradient, and crucible or crystal rotation has a profound influence on the interface shape, surface striations, defect density, and crystal integrity. There are a number of numerical, analytical and experimental works that simulate various aspects of these effects; see, for example, Laudise (1979), Carruthers (1977), Schwabe and Scharmann (1981), Simpkins and Dudderar (1981), Ostrach (1983), Simpkins and Chen (1985, 1986), Miller and Pernell (1981), and Simpkins (1981). However, the causes of misshapen and nonuniform crystal growth are still not well understood due to the complexity of the process.

The experimental studies of Miller and Pernell (1981) and Simpkins (1981) are of particular interest to this work. The first study involved heating the side walls of an open cylinder containing water. The authors characterized the flow into three regions when the temperature of the bottom wall is below that of the side walls. From the top to the bottom surfaces the regions are: (*i*) a thin surface layer; (*ii*) a convection region with essentially uniform temperature; and (*iii*) a motionless region, the so-called "stagnant" region. In a rectangular container with hot side walls and cooled top and bottom surfaces, Simpkins (1981) observed the appearance of two large recirculation cells, separated by a descending plume, in the upper portion of the container. The plume was fed by thin boundary layers adjacent to the vertical walls, and it would only sink to a critical depth in the container. Below this depth the flow was not strictly stagnant but moved very slowly relative to the motion in the upper layer. The top surfaces in these two works were free of motion and held at approximately constant temperatures. The experimental condition in Simpkins (1981) was for a Rayleigh number o(10^7) and aspect ratio o(1).

To complement the above experimental works, it is the purpose of this study to investigate numerically the buoyancy-driven flow in an enclosure in which the side-wall temperatures are higher than that of the bottom wall. The top wall is either rigid or represents a free surface, and is kept at an intermediate uniform temperature. Flow and heat transport in the recirculation cells, descending plume and stagnant layer, and the influence of free surface effects and asymmetric boundary conditions, are presented and discussed for $Pr = 7$, a Rayleigh number range 10^4 to 10^7, and aspect ratios (width/height) of 1 and 1.5. The calculated results compare fairly well with the available experimental data.

It should be noticed that the flow due to a heat source (such as a fire) located on the bottom wall of a symmetric enclosure strongly resembles (when inverted) the flow of interest here. For example, a detailed analysis has been performed by Rehm et al. (1982), but neglecting the molecular diffusion of momentum and heat which are crucial to this study. In contrast to the heat-source/plume configuration, the descending plume problem of interest here has received considerably less attention; see, for example, Simpkins and Chen (1985) and Simpkins (1985).

It is recognized that the practical realization of the present problem is bound to exhibit some degree of three dimensionality and unsteadiness. In this regard, the investigations of Humphrey and Bleinc (1985) and Simpkins (1985) are especially relevant. The top half of a vertical plate was cooled and the bottom half was heated by Humphrey and Bleinc (1985). This configuration induced boundary layer flows of opposing sign to collide halfway along the plate. The resulting flow was essentially two dimensional until Rayleigh numbers larger than 10^8 were imposed, at which point the motion in the collision region became three dimensional and unsteady, with time and length scales commensurate with the boundary layer

Contributed by the Heat Transfer Division and presented at the ASME Winter Annual Meeting, Anaheim, California, December 1986. Manuscript received by the Heat Transfer Division April 7, 1986.

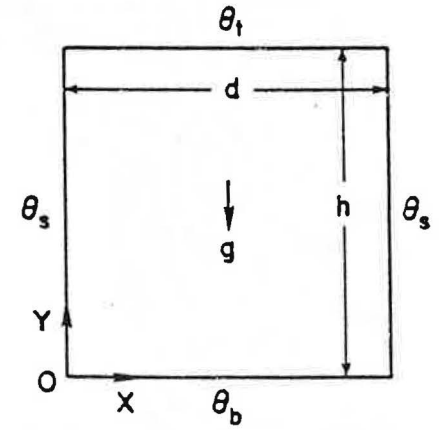

Fig. 1 Schematic of two-dimensional enclosure and coordinates. For the case of interest $\theta_s > \theta_t > \theta_b$.

length and time scales. In the present, more stable flow configuration, the maximum Rayleigh investigated was 10^7 and, therefore, the assumption of two-dimensional flow is not unrealistic.

Unsteadiness of the plume leaving the top surface of the enclosure where the turning boundary layers collide is discussed by Simpkins (1985). Measurements obtained by Simpkins (1985) in an enclosure of aspect ratio unity and $\mathrm{Ra} = 7 \times 10^6$ revealed a meandering plume of changing length. The periodicity determined was about 30 s for a value $(T_b - T_t)/(T_s - T_t) = -4.5$. Experimental attempts failed to stabilize the meandering of the collision region, and hence of the plume. In the present study $(T_b - T_t)/(T_s - T_t) = -2.39$ and, while we cannot rule out the possible meandering of a plume corresponding to our calculation conditions, its periodicity should be greater than 30 s. The results presented here were obtained with a time-dependent calculation scheme that evolved to steady state *without* displaying oscillatory motions of the type just described.

2 Governing Equations and Solution Procedure

Consider a two-dimensional rectangular enclosure filled with fluid, such as is shown in Fig. 1. The two side walls are maintained at the same temperature θ_s, while the top and bottom surfaces are kept at the lower temperatures θ_t and θ_b, respectively. Employing the Boussinesq approximation, the nondimensional equations describing laminar flow in stream function and vorticity form are

$$\frac{\partial \omega}{\partial \tau} + U\frac{\partial \omega}{\partial X} + V\frac{\partial \omega}{\partial Y} = \mathrm{Ra}\,\mathrm{Pr}\frac{\partial \theta}{\partial X} + \mathrm{Pr}\,\nabla^2\omega \tag{1}$$

$$\frac{\partial \theta}{\partial \tau} + U\frac{\partial \theta}{\partial X} + V\frac{\partial \theta}{\partial Y} = \frac{\partial^2 \theta}{\partial X^2} + \frac{\partial^2 \theta}{\partial Y^2} \tag{2}$$

$$\nabla^2\psi = -\omega \tag{3}$$

$$\frac{\partial \psi}{\partial Y} = U, \qquad \frac{\partial \psi}{\partial X} = -V \tag{4}$$

The initial and boundary conditions are

$$\tau = 0: \quad U = V = 0, \quad \theta = 0 \tag{5a}$$

$\tau > 0$:

$$X = 0 \text{ or } 1: \quad \psi = \frac{\partial \psi}{\partial X} = 0, \quad \theta = 1 \tag{5b}$$

$$Y = 0: \quad \psi = \frac{\partial \psi}{\partial Y} = 0, \quad \theta = 0 \tag{5c}$$

$$Y = AR: \quad \psi = \frac{\partial \psi}{\partial Y} = 0, \quad \theta = 0.7053 \quad \text{(rigid top surface)} \tag{5d}$$

$$\psi = \frac{\partial \psi}{\partial X} = 0, \quad \theta = 0.7053 \quad \text{(free top surface)} \tag{5e}$$

$$\omega = -\mathrm{Ma}\frac{\partial \theta}{\partial X} = 0 \quad \text{(free top surface)} \tag{5f}$$

Note that in this study $AR = 1$ or 1.5, and the top surface is kept at a temperature between that of the bottom and side walls. Equation (5*d*) is used if the top wall represents a rigid surface. In this case, the vorticity is calculated by linear extrapolation from two interior points adjacent to the boundary.

Nomenclature

AR = aspect ratio = h/d
d = width of cavity shown in Fig. 1
g = gravitational acceleration
h = height of cavity shown in Fig. 1
Ma = Marangoni number defined in equation (6)
Nu_s = mean value of Nusselt number on side wall, defined in equation (8)
Pr = Prandtl number = ν/α
q = average heat flux from side wall
Ra = Rayleigh number = $g\beta(T_s - T_b)d^3/\nu\alpha$
T = absolute temperature
u = velocity in x direction
U = dimensionless velocity in x direction = ud/α
v = velocity in y direction
V = dimensionless velocity in y direction = vd/α
x = horizontal coordinate shown in Fig. 1
X = dimensionless horizontal coordinate = x/d
y = vertical coordinate shown in Fig. 1
Y = dimensionless vertical coordinate = y/d
α = thermal diffusivity of fluid
β = thermal expansion coefficient of fluid
γ = surface tension gradient defined in equation (7)
δ = thermal layer thickness on the bottom wall
Δ = difference
θ = dimensionless temperature = $(T - T_b)/(T_s - T_b)$
μ = dynamic viscosity of fluid
ν = kinematic viscosity of fluid
σ = surface tension coefficient
τ = dimensionless time = $t\alpha/d^2$
ψ = dimensionless stream-function defined in equation (4)
ω = dimensionless vorticity defined in equation (3)
Ω = relaxation parameter

Superscripts

p = iteration number

Subscripts

b = bottom wall
i, j = subscripts denoting X and Y grid node
s = side wall
t = top wall

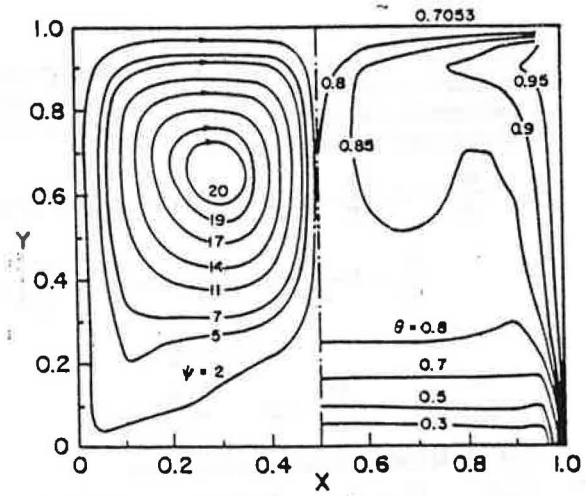

Fig. 2 Streamline and isotherm contours in an enclosure with $Ra = 10^6$, $AR = 1.0$, and rigid upper surface

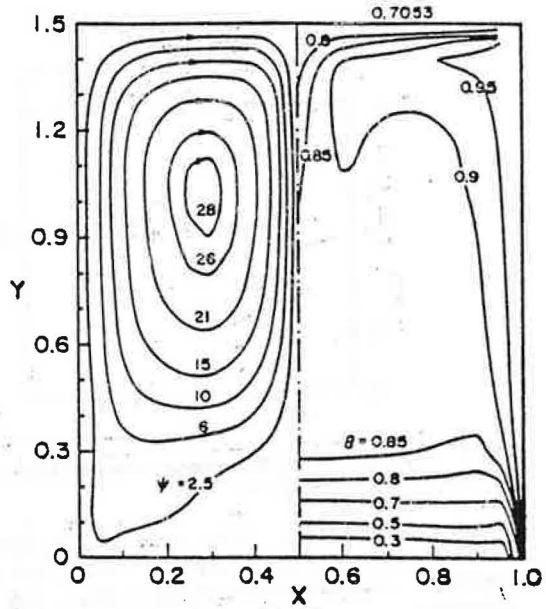

Fig. 3 Streamline and isotherm contours in an enclosure with $Ra = 10^6$, $AR = 1.5$, and rigid upper surface

Equations (5e, 5f) are used instead if the top wall represents a free surface. Ma in equation (5f) is the Marangoni number defined by

$$\mathrm{Ma} = -\frac{\gamma d \Delta T}{\alpha \mu} \tag{6}$$

where $\Delta T = T_s - T_b$. In the above equation γ is defined by

$$\gamma = -\frac{d\sigma}{dT} \tag{7}$$

where σ is surface tension of the fluid. The derivation of equation (5f) is given in the appendix. Since the free surface is held at constant temperature, surface tension gradients do not drive the flow and so the value of vorticity at the free surface vanishes.

Equations (1)–(5) are solved in the following manner. Given the field values at time $n\Delta\tau$, the vorticity and temperature at time $(n+1)\Delta\tau$ are calculated by the ADI method from equations (1) and (2), respectively, as described in Wilkes and Churchill (1966). The stream function is then computed from equation (3) using the successive overrelaxation (S.O.R.) method. Finally, the new values of U and V are computed by a central difference approximation to equation (4). 41 × 41 grid points are used for the case of aspect ratio 1, and 41 × 61 for the aspect ratio 1.5. This level of grid refinement guaranteed not fewer than 2 grid points within the side-wall boundary layers at the highest Rayleigh number investigated. In solving the stream function by the S.O.R. method, the convergence criterion within each time step is

$$\left| \frac{\psi_{ij}^{\rho+1} - \psi_{ij}^{\rho}}{\psi_{ij}^{\rho+1}} \right| \le 5.0 \times 10^{-5}$$

All the results presented here correspond to steady-state conditions. As in Wilkes and Churchill (1966), steady state is presumed to have been reached when

$$\left| \frac{\mathrm{Nu}_s^{\rho+1} - \mathrm{Nu}_s^{\rho}}{\mathrm{Nu}_s^{\rho+1}} \right| \le 5.0 \times 10^{-6}$$

where Nu_s is the average Nusselt number on the vertical side wall given by

$$\mathrm{Nu}_s = \left[\int_0^{AR} \left. \frac{\partial \theta}{\partial X} \right|_{X=0} dY \right] / AR \tag{8}$$

3 Results and Discussion

Prior to the calculations, numerical tests were conducted to check the accuracy of the ADI procedure by reference to the flow generated by differentially heating the side walls of a rectangular enclosure while keeping the top and bottom walls adiabatic. The results were compared with the benchmark solution of de Vahl Davis (1981). They are reported in Chen (1985) and substantiate the correctness of the numerical calculation procedure.

The computation time depends on the numerical time step $\Delta\tau$, the Rayleigh number, the number of grid points, and the S.O.R. parameter Ω. For a 41 × 41 grid, with $\Delta\tau = 2.0 \times 10^{-4}$ and $\Omega = 1.73$, the CPU time is approximately 4000 s on a CDC CYBER 170/815 when $Ra = 10^4$–10^6; and about 9000 s when $\Delta\tau = 1.0 \times 10^{-5}$ and $Ra = 10^7$.

Figure 2 shows the streamlines and isotherms for $Ra = 10^6$ and $AR = 1$ in an enclosure with a rigid upper surface. Along each side wall an upward flow is induced by natural convection. The two side-wall streams turn inward respectively at the top wall corners, flow along the top wall (to which they lose heat), and collide at $X = 0.5$. At this point the streams merge and "jet" or "plume" downward, along the symmetry plane of the enclosure. As the plume penetrates the bulk of the cooler fluid, it entrains fluid of increasing temperature. Heat is lost to the cold bottom surface as the plume descends further and splits into two streams each of which flows along the bottom wall, eventually to reach the side walls thus forming two recirculating cells.

The descending plume sinks to a critical depth of about $Y = 0.26$, below which the fluid is almost motionless. This layer of essentially motionless fluid is termed the stagnant layer by Miller and Pernell (1981). Figure 2 shows that the isotherms are almost parallel to the bottom surface in the stagnant layer and, therefore, that the heat transfer is conduction dominated.

Figure 3 shows corresponding results for $Ra = 1.0 \times 10^6$ and $AR = 1.5$. The resulting flow pattern is basically the same as for the previous case. However, the thermal boundary layer on the vertical wall is thinner and well developed. In addition, the temperature distribution is more uniform in the central portion of the enclosure, and the circulation strength in each cell is stronger, due to the increased heat transfer from the larger side walls.

Figure 4 shows the streamlines and isotherms for $Ra = 10^7$ and $AR = 1.0$, again for the case of a rigid upper surface. When compared with the case with $Ra = 10^6$ in Fig. 2, the results show that the circulation strength at $Ra = 10^7$ has

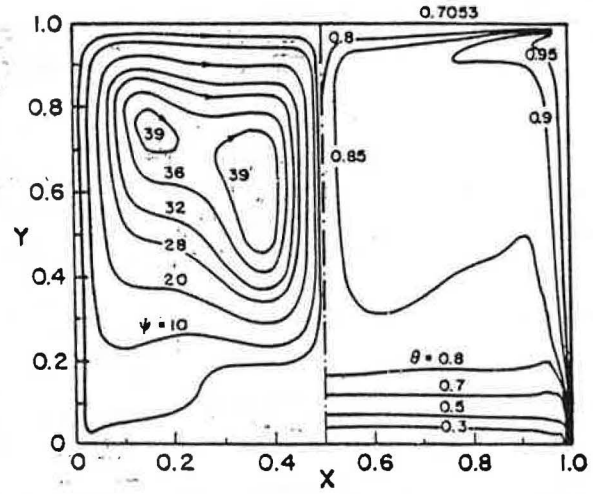

Fig. 4 Streamline and isotherm contours in an enclosure with $Ra = 10^7$, $AR = 1.0$, and rigid upper surface

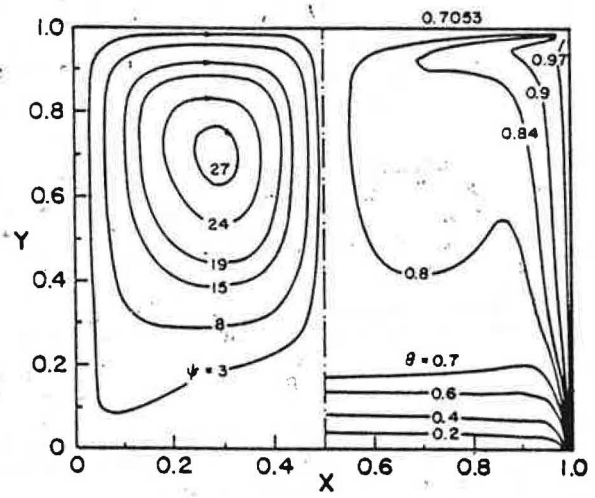

Fig. 5 Streamline and isotherm contours in an enclosure with $Ra = 10^6$, $AR = 1.0$, and free upper surface

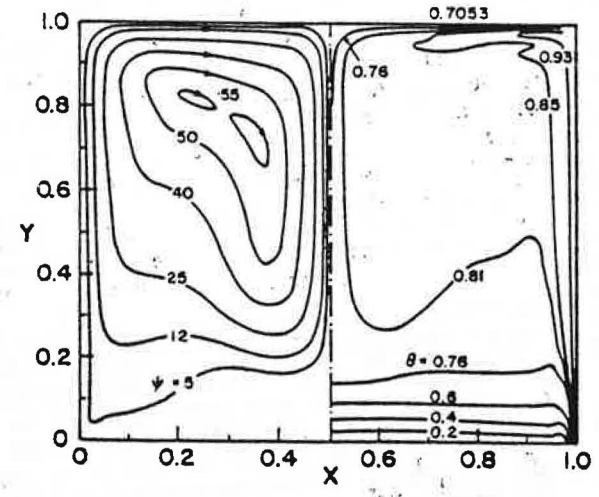

Fig. 6 Streamline and isotherm contours in an enclosure with $Ra = 10^7$, $AR = 1.0$, and free upper surface

almost doubled, due to the increased driving force. The strong circulation is accompanied by the appearance of a secondary eddy within each main cell.

To illustrate free surface effects, calculations were performed using the boundary conditions given by equations (5*e*) and (5*f*). Figures 5 and 6 show the resulting streamlines and isotherms for $Ra = 10^6$ and 10^7, respectively, with $AR = 1.0$. A comparison between the streamlines corresponding to Figs. 2 and 5 and Figs. 4 and 6 reveals that, for the same Ra and AR, the circulation strength is larger in the free surface case. This is especially noticeable at the higher Ra. In addition, the center of the circulation cell is displaced upward when the top surface is free to move. A comparison between the corresponding isotherms shows that the thermal boundary layers along the side and bottom walls for the free surface flow condition are thinner than those for a rigid surface condition.

None of the above cases displayed evidence of recirculation zones in the lower layer near each corner of the cavity as found by Simpkins (1985). While this may reflect a lack of sufficient grid refinement to calculate the flow in its full details, we note that the effect is very small (Simpkins, 1986) and is unlikely to alter substantially any of the conclusions of this work.

Figures 7 and 8 show vertical temperature profiles in a square enclosure at the center plane, $X = 0.5$, for $Ra = 10^4 - 10^7$, for rigid and free upper boundary conditions, respectively. These results confirm that the flow field is stably stratified in the bottom stagnant region and that as Ra increases the stagnant layer becomes thinner. The temperature in the enclosure center is essentially uniform, but an inversion arises near the top surface at higher Ra. These results are in good qualitative agreement with those observed experimental-

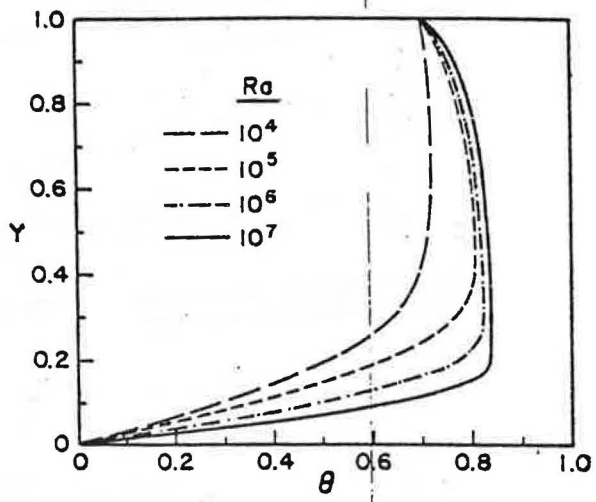

Fig. 7 Temperature profiles along the enclosure height at the center plane, $X = 0.5$, for various Rayleigh numbers (rigid upper surface)

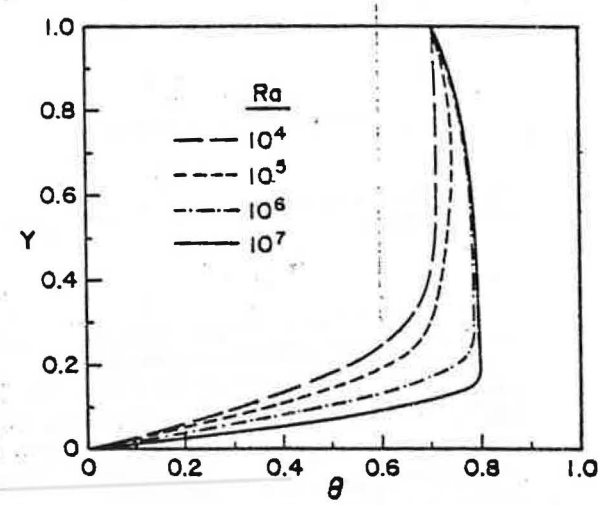

Fig. 8 Temperature profiles along the enclosure height at the center plane, $X = 0.5$, for various Rayleigh numbers (free upper surface)

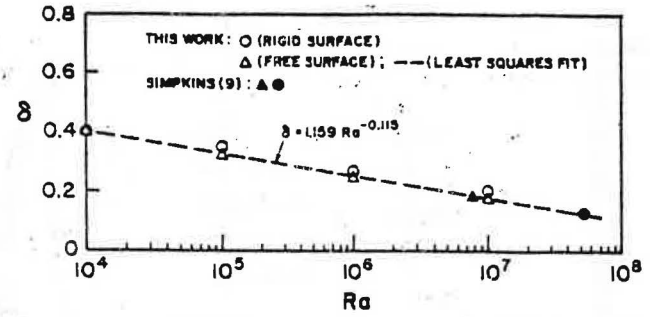

Fig. 9 Thermal layer thickness on the bottom wall of an enclosure with $AR = 1$ as function of Rayleigh number

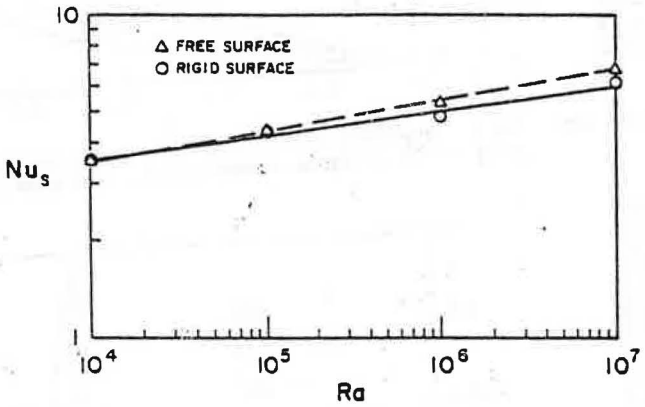

Fig. 10 Average Nusselt number on the side wall as function of Rayleigh number

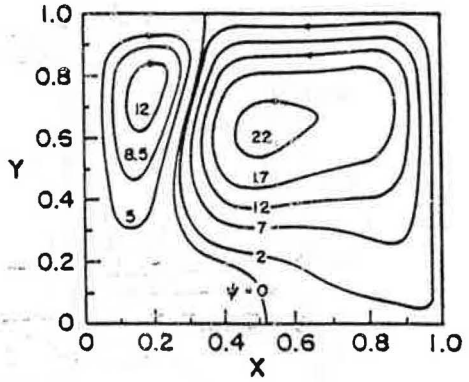

Fig. 11(a) Streamline contours in an enclosure with $Ra = 10^6$, $AR = 1.0$, and rigid upper surface

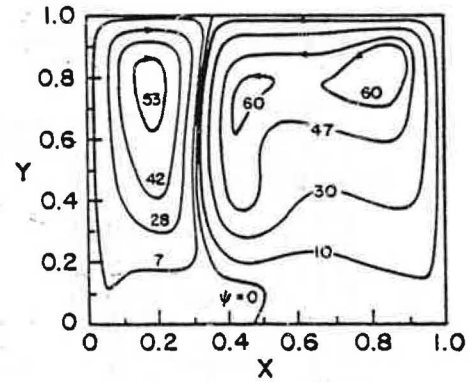

Fig. 11(b) Streamline contours in an enclosure with $Ra = 10^7$, $AR = 1.0$, and free upper surface

ly by Simpkins (1981), who performed experimental observations in enclosures with a free upper surface.

The influence of the free surface is also exhibited in Fig. 8, when compared with Fig. 7. The comparison shows that: (*i*) The temperature inversion near the upper surface becomes smaller; (*ii*) the temperature is more uniformly distributed; and (*iii*) the bottom thermal layer becomes thinner, in the free surface case. These results are consistent with the stronger circulation strength observed for the free upper surface condition.

The bottom layer thickness δ versus Ra is presented in Fig. 9 for both rigid and free upper boundaries, together with the experimental data from Simpkins (1981). It can be seen that δ decreases with Rayleigh number according to $Ra^{-0.115}$. The predictions for the free surface condition compare very well with the experimental findings by Simpkins (1981) even though the upper surface boundary conditions do not correspond exactly. Unfortunately, it has not been possible to conduct similar detailed comparisons of velocity and temperature profiles with the results of others. In the case of velocity, the data are simply unavailable; although we note that in Simpkins (1985) there is a reference to forthcoming measurements. Data for temperature have been reported by Miller and Pernell (1981) and Simpkins (1981) but, because the configurations and/or aspect ratios investigated differ from those of this study, exact comparisons cannot be made.

The mean Nusselt number of a vertical side wall Nu_s is shown as a function of Ra in Fig. 10. The results show that Nu_s for the free surface case is larger than that for the rigid. The following correlations were derived from the calculations:

$$Nu_s = 1.43\ Ra^{0.097} \text{ (free upper surface)} \quad (9)$$

$$Nu_s = 1.75\ Ra^{0.077} \text{ (rigid upper surface)} \quad (10)$$

Numerical experiments were performed to investigate the sensitivity of the flow in the enclosure to an asymmetric

Table 1 Calculated values of side-wall Nusselt number for symmetric and asymmetric side-wall temperature boundary conditions

Ra	Boundary Condition	Rigid Upper Surface: left (colder) wall	Rigid Upper Surface: right (hotter) wall	Free Upper Surface: left (colder) wall	Free Upper Surface: right (hotter) wall
10^4	Sym.	3.5409	3.5408	3.5408	3.5406
	Asym.	3.5264	4.2631	3.5267	4.2645
	(%)	(-0.41)	(20.4)	(-0.45)	(20.4)
10^5	Sym.	4.3244	4.3245	4.3578	4.3579
	Asym.	3.7830	4.9424	3.9458	5.1520
	(%)	(-12.5)	(14.3)	(-9.5)	(18.2)
10^6	Sym.	4.8472	4.8472	5.3099	5.3099
	Asym.	4.4345	6.2594	4.9722	6.8987
	(%)	(-8.5)	(29)	(-6.4)	(30)
10^7	Sym.	6.1432	6.1432	6.9755	6.9757
	Asym.	5.4262	8.3123	6.5339	9.5109
	(%)	(-12)	(35)	(-6.3)	(36)

specification of the side-wall boundary conditions. This was readily accomplished by fixing $\theta_s = 1.1$ on the right-hand side of the enclosure shown in Fig. 1 while specifying the remaining boundary conditions as explained above. Figure 11(*a*) illustrates the extent and magnitude of the artificially induced asymmetry for the case $Ra = 10^6$ in a square enclosure with a rigid upper surface. Qualitatively similar flow patterns were observed at the other values of Ra, irrespective of whether the top boundary was a rigid or free-moving surface. However, at $Ra = 10^7$ the free-moving surface case displayed the interesting eddy structure shown in Fig. 11(*b*). Comparing with the streamlines shown in Fig. 6, it is seen that the effect of the asymmetry is to intensify the motion of the secondary eddy in the main right-hand cell, while eliminating the secondary eddy in the main left-hand cell. The corresponding effect of the asymmetry on the temperature fields, in square enclosures

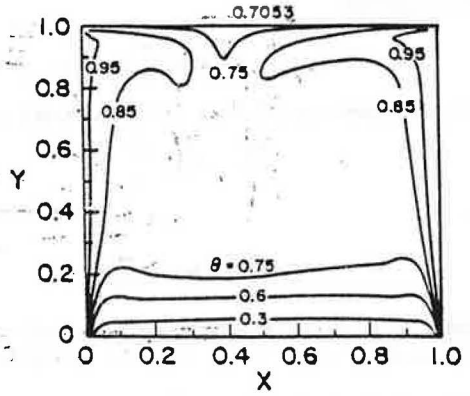

Fig. 12(a) Isotherm contours in an enclosure with $Ra = 10^6$, $AR = 1.0$, and rigid upper surface

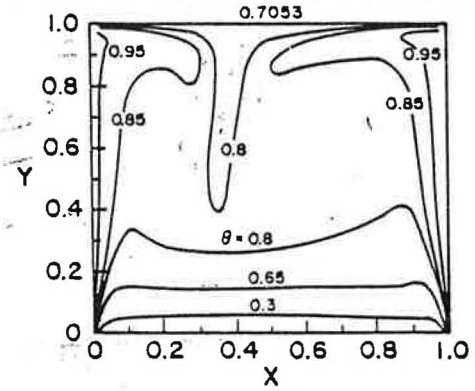

Fig. 12(b) Isotherm contours in an enclosure with $Ra = 10^6$, $AR = 1.0$, and free upper surface

with rigid and free-moving top surfaces, respectively, is shown in Figs. 12(*a*, *b*) for $Ra = 10^6$.

Table 1 presents calculated values of side-wall Nusselt numbers for conditions corresponding to symmetric and asymmetric specifications of the side-wall temperatures. In all cases, irrespective of whether the top surface is rigid or free, the hotter side wall experiences a proportionately larger increase in Nu_r than the corresponding decrease experienced by the cooler side wall. (That this is the case is readily seen from the percentage changes shown in parentheses in the table.) The table also shows that between $Ra = 10^4$ and 10^5 the *rate of increase* in Nu_r on the hotter side wall, induced by the asymmetry, is substantially reduced (20.4 percent to 14.3 percent for an enclosure with rigid upper surface) but that it is restored to high values at $Ra = 10^6$ and 10^7 (29 percent, 35 percent). A corresponding but less substantial variation is shown by the cooler wall between $Ra = 10^5$ and 10^6, where the *rate of decrease* in Nu_r is temporarily reduced. The interpretation of this finding is complicated, due to the interactions that arise between the flow in each main cell and the portions of the horizontal boundaries with which each cell is in contact. This question is the subject of continuing research by one of us (JACH) in a related experiment at the University of California, Berkeley.

4 Conclusions

A numerical study was conducted for conditions of natural convection in a rectangular enclosure in which the side walls are hotter than the top wall, and the top wall is hotter than the bottom wall. Symmetric and asymmetric side-wall boundary conditions for temperature were considered. Calculations were performed for $Ra = 10^4$ to 10^7, and $AR = 1.0$ and 1.5. Two enclosure configurations, one with a rigid top wall, the other with a free-moving fluid surface, were investigated. Comparisons between the calculations and limited experimental data show good agreement. The following major conclusions can be drawn from this study:

1 Steady-state, two-dimensional, numerical simulations indicate that there are two regions in the flow field of the enclosure configuration studied. In the upper part, two large cells separated by a descending plume circulate in mutually counterrotating directions. The plume sinks to a limited depth, below which lies a fluid layer that is essentially motionless.

2 Temperature profiles along the cavity height at the midplane, $X = 0.5$, indicate that the bottom layer of fluid in the enclosure is stably stratified. In the enclosure center, the fluid temperature is essentially uniform, due to strong mixing by the recirculating cells. A temperature inversion, especially strong at high Ra, occurs near the top layer.

3 When the aspect ratio increases at a fixed Ra, the circulation strength increases, with thinner boundary layers arising along the vertical side walls of the enclosure.

4 At high Rayleigh number, e.g., $Ra = 10^7$, the circulation strength increases and a secondary eddy develops within each of the two larger main cells filling the enclosure.

5 The thickness of the stratified fluid layer in the bottom of the enclosure varies with Rayleigh number according to $\delta = 1.159\ Ra^{-0.115}$.

6 For equal Ra and AR, the free surface enclosure flow reveals: (1) larger circulation strength; (2) higher heat transfer rates; and (3) smaller bottom layer thickness, relative to the rigid surface case.

7 The flow and heat transfer in the enclosure are strongly affected by an asymmetric specification of the side-wall temperatures. The asymmetry induces a disproportionately higher increase in the Nusselt number of the hotter side wall relative to the decrease in Nusselt that arises at the colder side wall.

Acknowledgments

One of us (JACH) gratefully acknowledges the financial support provided by the Department of Energy under grant No. DE-FG03-85ER13397. We are grateful to Ms. Loris C-H. Donahue for the typing of this manuscript. The authors' names are listed in alphabetical order.

References

Carruthers, J. R., 1977, *Preparation and Properties of Solid State Materials*, Wilcox and Lefever, eds., Marcel Dekker, New York, Vol. 3.

Chen, K. S., 1985, "The Heat Transfer Study in Czochralski Crystal Growth," Mid-term report to National Science Council, NSC-74-0401-E110-06, Taiwan, ROC.

de Vahl Davis, G., 1981, "Natural Convection of Air in a Square Cavity: An Accurate Numerical Solution," Report 1981/FMT/1, University of N.S.W., Kensington, Australia.

Humphrey, J. A. C., and Bleinc, C., 1985, "On the Structure of the Flow Due to the Collision of Opposed, Vertical, Free Convection, Boundary Layers," *Int. Comm. Heat and Mass Transfer*, Vol. 12, pp. 233–240.

Hurle, D. T. J., 1977, "Hydrodynamics in Crystal Growth," in: *Crystal Growth and Materials*, E. Kaldis and H. J. Scheel, eds., North Holland, Vol. 2, pp. 549–569.

Laudise, R. A., 1970, *The Growth of Single Crystals*, Prentice-Hall Inc., New York.

Miller, D. L., and Pernell, T. L., 1981, "The Temperature Distribution in a Simulated Garnet Czochralski Melt," *J. Crystal Growth*, Vol. 53, pp. 523–529.

Ostrach, S., 1982, "Low Gravity Fluid Flows," *Ann. Rev. Fluid Mech.*, M. Van Dyke, J. V. Wehausen, and J. L. Lumley, eds., Annual Reviews Inc., Vol. 14, pp. 313–345.

Ostrach, S., 1983, "Fluid Mechanics in Crystal Growth – The 1982 Freeman Scholar Lecture," *J. Fluid Engrg.*, Vol. 105, pp. 5–20.

Rehm, R. G., Baum, H. R., and Barnett, P. D., 1982, "Buoyant Convection Computed in a Vorticity, Stream-Function Formulation," *J. of Res.*, Nat. Bur. Stand., Vol. 87, No. 2, pp. 165–185.

Schwabe, D., and Scharmann, A., 1981, "Marangoni Convection in Open Boat and Crucible," *J. Crystal Growth*, Vol. 52, pp. 435–449.

Simpkins, P. G., 1981, "On Descending Plumes in Containers," *Bulletin Am. Phys. Soc.*, Vol. 26, No. 8, p. 1277.

Simpkins, P. G., and Dudderar, T. D., 1981, "Convection in Rectangular

Cavities With Differentially Heated End Walls," *J. Fluid Mech.*, Vol. 110, pp. 433–456.

Simpkins, P. G., and Chen, K. S., 1985, "Natural Convection in Horizontal Containers With Applications to Crystal Growth," In: *Natural Convection: Fundamentals and Applications*, S. Kakac, W. Aung, and R. Viskanta, eds., Hemisphere Publishing Corporation, Washington, DC.

Simpkins, P. G., 1985, "Convection in Enclosures at Large Rayleigh Numbers," in: *Stability in Convective Flows*, W. S. Saric and A. A. Szewczyk, eds., ASME, HTD-Vol. 54, pp. 39–47.

Simpkins, P. G., and Chen, K. S., 1986, "Convection in Horizontal Cavities," *J. Fluid Mech.*, Vol. 166, pp. 21–39.

Simpkins, P. G., 1986, Personal Communication.

Villers, D., and Platten, J. K., 1985, "Marangoni Convection in Systems Presenting a Minimum in Surface Tension," *Physico-Chemical Hydrodynamics*, Vol. 6, No. 4, pp. 435–451.

Wilkes, J. O., and Churchill, S. W., 1966, "The Finite-Difference Computation of Natural Convection in a Rectangular Enclosure," *AIChE J.*, Vol. 12, pp. 161–166.

APPENDIX

For a free fluid surface subjected to a temperature gradient, the shear stress along the surface is balanced by the surface tension gradient according to Ostrach (1982) and Villers and Platten (1985)

$$\mu \frac{\partial u}{\partial y} = \frac{\partial \sigma}{\partial x} = \frac{\partial \sigma}{\partial T} \frac{\partial T}{\partial x} \tag{A1}$$

The nondimensional form of the above equation is

$$\frac{\partial U}{\partial Y} = \mathrm{Ma} \frac{\partial \theta}{\partial X} \tag{A2}$$

or

$$\frac{\partial^2 \psi}{\partial Y^2} = \mathrm{Ma} \frac{\partial \theta}{\partial X} \tag{A3}$$

where Ma is the Marangoni number defined by equation (6) in the text. Since $V = 0$ and $\partial \psi / \partial X = 0$ at the free surface, so also

$$\frac{\partial^2 \psi}{\partial X^2} = 0 \tag{A4}$$

Substitution of equations (A3) and (A4) into equation (3) yields equation (5*f*) in the text.